

MAXIMUM ENTROPY ON THE MEAN: A PARADIGM SHIFT FOR REGULARIZATION IN IMAGE DEBLURRING

GABRIEL RIOUX, RUSTUM CHOKSI, TIM HOHEISEL AND CHRISTOPHER SCARVELIS

ABSTRACT. Image deblurring is a notoriously challenging ill-posed inverse problem. In recent years, a wide variety of approaches have been proposed based upon regularization at the level of the image or on techniques from machine learning. We propose an alternative approach, shifting the paradigm towards regularization at the level of the probability distribution on the space of images. Our method is based upon the idea of maximum entropy on the mean wherein we work at the level of the probability density function of the image whose expectation is our estimate of the ground truth. Using techniques from convex analysis and probability theory, we show that the method is computationally feasible and amenable to very large blurs. Moreover, when images are imbedded with symbology (a known pattern), we show how our method can be applied to approximate the unknown blur kernel with remarkable effects. While our method is stable with respect to small amounts of noise, it does not actively denoise. However, for moderate to large amounts of noise, it performs well by preconditioned denoising with a state of the art method.

1. INTRODUCTION

Ill-posed inverse problems permeate the fields of image processing and machine learning. Prototypical examples stem from the non-blind (deconvolution) and blind deblurring of digital images. The vast majority of methods for image deblurring are based on some notion of regularization (eg. gradient based) at the image level. Motivated by our previous work [19] for bar codes, we address general image deblurring at the level of the probability density function of the ground truth. Using Kullback-Leibler divergence as our regularizer, we present a novel method for both deconvolution and kernel (point spread function) estimation via the expectation of the probability density with maximum entropy. This higher-level approach is known in information theory as *maximum entropy on the mean* and dates back to E.T. Jaynes in 1957 [8, 9]. Our approach is made computationally tractable as a result of two observations:

- (i) Fenchel-Rockafellar duality transforms our infinite-dimensional primal problem into a finite-dimensional dual problem;
- (ii) The sought expectation of the maximal probability distribution can be simply written in terms of known moment generating functions and the optimizer of the dual problem.

What is particularly remarkable about our higher-level method is that it effectively restores images that have been subjected to significantly greater levels of blur than previously considered in the literature. While the method is stable with respect to small amounts of noise, it does not actively denoise; however, for moderate to large amounts of noise, it can readily be preconditioned by first applying expected patch log likelihood (EPLL) denoising [28].

We test and compare our method on a variety of examples. To start, we present an example of simple deconvolution (without additive noise) but for a range of blurs for which previous methods do not even converge (cf. Fig. 1). Then we consider deconvolution with small to significant additive noise. We show that we can precondition with EPLL denoising to attain deconvolution results comparable with the state of the art (cf. Fig. 3). We then address blind deblurring with the inclusion of a known shape (analogous to a finder pattern in a QR bar codes [19]). In these cases, we can, preconditioning with EPLL denoising, blindly deblur with large blurs (cf. Figs. 4, 5, 6). Given that our method relies on symbology, comparison with other methods is unfair (in our favour). However, we do provide comparison with the state of the art method of Pan et al. [16, 15] to demonstrate the power of our method in exploiting the symbology (finder pattern) to accurately recover the blur (point spread function).

Overall, we introduce a novel regularization method which is theoretically well-founded, numerically tractable, and amenable to substantial generalization. While we have directly motivated and applied our higher-level regularization approach to image deblurring, we anticipate that it will also prove useful in solving other ill-posed inverse problems in computer vision, pattern recognition and machine learning.

2. CURRENT METHODS

The process of capturing one channel of a blurred image $b \in \mathbb{R}^{n \times m}$ from a ground truth channel $x \in \mathbb{R}^{n \times m}$ is modelled throughout by the relation $b = c * x$, where $*$ denotes the 2-dimensional convolution between the kernel $c \in \mathbb{R}^{k \times k}$ ($k < n, m$) and the ground truth; this model represents spatially invariant blurring. For images composed of more than one channel, blurring is assumed to act on a per-channel basis. We therefore derive a method to deblur one channel and apply it to each channel separately.

Current blind deblurring methods consist of solving

$$(1) \quad \inf_{\substack{x \in \mathbb{R}^{n \times m} \\ c \in \mathbb{R}^{k \times k}}} \left\{ \frac{\alpha}{2} \|c * x - b\|_2^2 + R(x, c) \right\},$$

where $R : \mathbb{R}^{n \times m} \times \mathbb{R}^{k \times k} \rightarrow \mathbb{R}$ serves as a regularizer which permits the imposition of certain constraints on the optimizers. This idea of regularization to solve ill-posed inverse problems dates back to Tikhonov [26]. Approaches that are not based on machine learning differ mostly on the choice of regularizer, examples include L_0 -regularization, which penalizes the presence of non-zero pixels in the image or gradient [15]; weighted nuclear norm regularization, which ensures that the image or gradient matrices have low rank [18] and L_0 -regularization of the dark channel, which promotes sparsity of a channel consisting of local minima in the intensity channel [16]. As it pertains to machine learning methods, other approaches have been employed including modelling the optimization problem as a deep neural network [24] and estimating the ground truth image from a blurred input without estimating the kernel using convolutional neural networks [13, 14, 25] or generative adversarial networks [11, 17].

The results achieved in these papers are comparable to the state of the art. However, to our knowledge, such methods have not been successfully applied to the large blurring regimes considered in this paper. Our method presents a paradigm shift in image deblurring by optimizing at the level of the set of probability densities rather than the set of images.

3. OUR METHOD

3.1. Kullback-Leibler Regularized Deconvolution. We first describe the method for the case of deconvolution and begin by establishing some notation and definitions. The convolution operator $c*$ will be denoted by the matrix $C : \mathbb{R}^d \rightarrow \mathbb{R}^d$ acting on a vectorized image $x \in \mathbb{R}^d$ for $d = nm$ and resulting in a vectorized blurred image for which the k^{th} coordinate in \mathbb{R}^d corresponds to the k^{th} pixel of the image.

The expectation $\mathbb{E}_\rho[\mathbf{X}]$ of a random vector $\mathbf{X} = [X_1, \dots, X_d]^T$ on $\Omega \subset \mathbb{R}^d$ associated with a probability measure $\rho \in \mathcal{P}(\Omega)$, the set of probability measures on Ω , is a vector whose k^{th} component is given by $(\mathbb{E}_\rho[\mathbf{X}])_k = \int_\Omega x_k d\rho(x)$.

Letting $\rho, \mu \in \mathcal{P}(\Omega)$, we write $\rho \ll \mu$ to denote that ρ is absolutely continuous with respect to μ , i.e. if $A \subseteq \Omega$ is such that $\mu(A) = 0$, then $\rho(A) = 0$. Notably, if μ is in turn absolutely continuous with respect to the Lebesgue measure dx then $\mu = q(x)dx$ and $\rho = p(x)dx$. In this context, we denote by $\mathcal{K}(\rho, \mu)$ the Kullback-Leibler divergence between ρ and μ , i.e.

$$(2) \quad \mathcal{K}(\rho, \mu) = \begin{cases} \int_\Omega \log \left(\frac{p(x)}{q(x)} \right) p(x) dx, & \rho \ll \mu, \\ +\infty, & \text{otherwise.} \end{cases}$$

Given $b \in \mathbb{R}^d$ and $\Omega \in \mathbb{R}^d$ compact, we wish to determine the optimizer of

$$(3) \quad \inf_{\rho \in \mathcal{P}(\Omega)} \left\{ \frac{\alpha}{2} \|c * \mathbb{E}_\rho[\mathbf{X}] - b\|_2^2 + \mathcal{K}(\rho, \mu) \right\}.$$

In this framework, the expectation of this optimizer is taken to be the estimate of the ground truth. Throughout, μ will be chosen to admit a density q with respect to the Lebesgue measure dx and ρ to admit a density p .

In its current form Eq. 3 is an infinite-dimensional optimization problem with no obvious solution and is thus intractable. In the sequel, a corresponding finite-dimensional dual problem will be established which will, along with a method to recover the expectation of solutions of Eq. 3 from solutions of this dual problem, permit a relatively fast and remarkably accurate estimation of the original image.

3.2. Dual Problem. In order to derive the (Fenchel-Rockafellar) dual problem to Eq. 3 we provide the reader with the Fenchel-Rockafellar duality theorem in a form expedient for our study, cf. e.g. [27, Cor. 2.8.5].

Theorem 1 (Fenchel-Rockafellar Duality Theorem). *Let X and Y be locally convex spaces and let X^* and Y^* denote their dual spaces. Moreover, let $f : X \rightarrow \mathbb{R} \cup \{+\infty\}$ and $g : Y \rightarrow \mathbb{R} \cup \{+\infty\}$ be convex, lower semicontinuous¹ and proper functions and let A be a continuous linear operator from X to Y . Assume that there exists $\bar{x} \in A \text{ dom } f \cap \text{dom } g$ such that g is continuous at $A\bar{x}$. Then*

$$(4) \quad \inf_{x \in X} \{f(x) + g(-Ax)\} = \max_{y^* \in Y^*} \{-f^*(A^*y^*) - g^*(y^*)\}$$

with A^* denoting the adjoint of A and f^* denoting the convex conjugate of f (cf. [27, Eq. 2.30]). Moreover, if \bar{y}^* is optimal in the maximization problem then

$$\bar{x} \in \partial f^*(A^*\bar{y}^*) = \operatorname{argmax}_{x \in X} \{(x, A^*\bar{y}^*) - f(x)\}$$

¹For convex functions, lower semicontinuity is equivalent to weak lower semicontinuity (cf. [27, Thm. 2.2.1])

is optimal in the minimization problem.

Proof. For the general statement and proof thereof, see [27, Cor. 2.8.5]. The theorem has been particularized to our application by using the following properties:

- (1) If $f : X \rightarrow \mathbb{R} \cup \{+\infty\}$ is convex, proper and lower semicontinuous, then $x^* \in \partial f(x)$ if and only if $x \in \partial f^*(x^*)$ [27, Thm. 2.4.4 (iv)].
- (2) If $f : X \rightarrow \mathbb{R} \cup \{+\infty\}$ is convex and proper then $\bar{x} \in \text{dom } f$ minimizes f if and only if $0 \in \partial f(\bar{x})$ [27, Thm. 2.5.7].

□

The equation in the last line of the theorem is known as the primal-dual recovery formula.

A particularly useful case of this theorem is when A is an operator between an infinite-dimensional locally convex space X and \mathbb{R}^d , as the dual problem will be a finite-dimensional maximization problem. Moreover, the primal-dual recovery is easy if f^* is differentiable, in which case the subdifferential equals the gradient. Some points must be clarified before we can apply this theorem.

First, $\mathcal{P}(\Omega)$ is not a locally convex space, but is a subset of the Banach space of regular complex Borel measures $\mathcal{M}(\Omega)$. The Riesz representation theorem [23, Thm. 6.19] states that the dual space of $(C_0(\Omega), \|\cdot\|_{L^\infty})$ is the space $(\mathcal{M}(\Omega), \|\cdot\|_{TV})$. Furthermore, the corresponding duality pairing $(\cdot, \cdot) : C_0(\Omega) \times \mathcal{M}(\Omega) \rightarrow \mathbb{R}$ is given by $(\psi, \eta) = \int_{\Omega} \psi d\eta$.

The constraint that $\rho \in \mathcal{P}(\Omega)$ in Eq. 3 can therefore be enforced by optimizing over $\mathcal{M}(\Omega)$ and adding the following indicator function

$$(5) \quad \delta(\rho | \mathcal{P}(\Omega)) = \begin{cases} 0, & \rho \in \mathcal{P}(\Omega), \\ +\infty, & \text{otherwise,} \end{cases}$$

to the objective function.

In the spirit of Thm. 1, we define

$$(6) \quad f = \mathcal{K}(\cdot, \mu) + \delta(\cdot | \mathcal{P}(\Omega)), \quad g = \frac{\alpha}{2} \|\cdot + b\|_2^2.$$

The convex conjugates of these functions are provided in the following two lemmas.

Lemma 1. *The function f defined in Eq. 6 is proper, lower semicontinuous and strictly convex. Moreover, $f^* : C_0(\Omega) \rightarrow \mathbb{R} \cup \{+\infty\}$ is given by the mapping $\psi \mapsto \log((\exp(\psi), \mu))$ and for any $\psi \in C_0(\Omega)$, for*

$$(7) \quad \bar{\rho}_\psi = \frac{\exp(\psi(x))q(x)}{\int_{\Omega} \exp(\psi(x))q(x) dx} dx$$

we have $\text{argmax}_{\rho \in \mathcal{M}(\Omega)} \{(\psi, \rho) - f(\rho)\} = \{\bar{\rho}_\psi\}$.

Proof. It is trivial to check that $\mathcal{P}(\Omega)$ is nonempty, closed and convex; hence its indicator function is proper, lower semicontinuous and convex. By [5, Thm. 3.2.17] $\mathcal{K}(\cdot, \mu)$ is proper and lower semicontinuous on $\mathcal{P}(\Omega)$. It is furthermore strictly convex since for every $t \in (0, 1)$ taking $\rho_1, \rho_2 \ll \mu$ with densities p_1, p_2 and $p_1 \neq p_2$, letting $p_t(x) = tp_1(x) + (1-t)p_2(x)$, one

has

$$\begin{aligned} \log \left(\frac{p_t(x)}{tq(x) + (1-t)q(x)} \right) p_t(x) &< tp_1(x) \log \left(\frac{p_1(x)}{q(x)} \right) \\ &+ (1-t)p_2(x) \log \left(\frac{p_2(x)}{q(x)} \right) \end{aligned}$$

where the strict log sum inequality [4, Thm. 2.7.1] has been used since p_1 and p_2 cannot simultaneously be equal to q and thus equality cannot hold. Integrating on both sides demonstrates strict convexity of the divergence, so f is strictly convex.

The convex conjugate is computed as follows

$$\begin{aligned} f^*(\psi) &= \sup_{\rho \in \mathcal{M}(\Omega)} \{(\psi, \rho) - \mathcal{K}(\rho, \mu) - \delta(\rho | \mathcal{P}(\Omega))\} \\ &= \sup_{\rho \in \mathcal{P}(\Omega)} \{(\psi, \rho) - \mathcal{K}(\rho, \mu)\} \\ &= \sup_{\substack{\rho \in \mathcal{P}(\Omega), \\ \rho \ll \mu}} \left\{ \int_{\Omega} \log \left(\exp(\psi(x)) \frac{q(x)}{p(x)} \right) p(x) dx \right\}. \end{aligned}$$

Since Ω is compact, $C_0(\Omega) \subseteq L^1(\Omega, \rho)$, as $\psi \in C_0(\Omega)$ is bounded and $p(x)$ integrates to 1 hence $|(\psi, \rho)| \leq \|\psi\|_{L^\infty(\Omega)}$. Thus, $\exp \psi \in L^1(\Omega, \rho)$ and since $-\log$ is a convex function, Jensen's inequality [23, Thm. 3.3] yields

$$(8) \quad f^*(\psi) \leq \log \left(\int_{\Omega} \exp(\psi(x)) q(x) dx \right).$$

This upper bound is attained by the probability measure

$$(9) \quad \bar{\rho} = \bar{p}(x) dx = \frac{\exp(\psi(x)) q(x)}{\int_{\Omega} \exp(\psi(x)) q(x) dx} dx,$$

which is admissible in the optimization problem defining the convex conjugate; hence

$$\log((\exp(\psi), \mu))$$

is indeed the convex conjugate of f . One notes that $\bar{\rho}$ is the unique maximizer since f is strictly convex [27, Prop. 2.5.6]. \square

Lemma 2. *The function g defined in Eq. 6 is proper, convex and continuous on \mathbb{R}^d . Its convex conjugate is given by $\frac{1}{2\alpha} \|\cdot\|_2^2 - \langle b, \cdot \rangle$.*

Proof. It is trivial to verify that this function is proper, convex and continuous. The conjugate can be determined by noting that $\frac{1}{2} \|\cdot\|_2^2$ is self-conjugate [20, Ex. 11.11] and applying standard properties of conjugacy [20, Eqn. 11(3)]. \square

Finally, we demonstrate that the expectation operator is of the proper form to apply the duality theorem.

Lemma 3. *Let $\Omega \in \mathbb{R}^d$ be compact, then the operator $\mathbb{E}_{(\cdot)}[\mathbf{X}] : \mathcal{M}(\Omega) \rightarrow \mathbb{R}$ is linear and continuous, moreover its adjoint is given by the mapping $z \in \mathbb{R}^d \mapsto \langle z, \cdot \rangle \in C_0(\Omega) \subseteq C_0(\Omega)^{**}$.*

Proof. Let $\rho, \eta \in \mathcal{M}(\Omega)$, linearity follows trivially from the definition of this functional. Next, continuity can be established as follows

$$(10) \quad \|\mathbb{E}_\rho[\mathbf{X}]\|_2^2 = \sum_{i=1}^d \left(\int_{\Omega} x_i d\rho(x) \right)^2 \leq \text{cst} \cdot \|\rho\|_{TV(\Omega)}^2$$

where the constant is given by $\sum_{i=1}^d \|x_i\|_{L^\infty(\Omega)}^2$. Thus, this operator is bounded and hence continuous. Letting $z \in \mathbb{R}^d$ be arbitrary, the adjoint can be computed as follows

$$(11) \quad \langle \mathbb{E}_\rho[\mathbf{X}], z \rangle = \sum_{i=1}^d z_i \int_{\Omega} x_i p(x) dx = \int_{\Omega} \langle z, x \rangle p(x) dx,$$

thus $\langle \mathbb{E}_\rho[\mathbf{X}], z \rangle = (\langle z, \cdot \rangle, \rho)$. \square

We can now state the main duality result.

Theorem 2. *Provided μ is absolutely continuous with respect to the Lebesgue measure, the dual problem to Eq. 3 is given by*

$$(12) \quad \max_{\lambda \in \mathbb{R}^d} \left\{ \langle b, \lambda \rangle - \frac{1}{2\alpha} \|\lambda\|_2^2 - \log \left(\int_{\Omega} \exp \langle C^T \lambda, x \rangle q(x) dx \right) \right\}.$$

Given a maximizer $\bar{\lambda}$ one can recover a minimizer of Eq. 3 via

$$(13) \quad \bar{\rho} = \bar{p}(x) dx = \frac{q(x) \exp \langle C^T \bar{\lambda}, x \rangle}{\int_{\Omega} \exp \langle C^T \bar{\lambda}, x \rangle q(x) dx} dx.$$

Proof. The dual problem can be obtained by applying the Fenchel-Rockafellar duality theorem (Thm. 1) with f and g defined in Eq. 6 to the following primal problem

$$\inf_{\rho \in \mathcal{M}(\Omega)} \left\{ \mathcal{K}(\rho, \mu) + \delta(\rho | \mathcal{P}(\Omega)) + \frac{\alpha}{2} \|b - C\mathbb{E}_\rho[\mathbf{X}]\|_2^2 \right\}$$

and substituting the expressions obtained in Lem. 1, 2 and 3, keeping in mind that the adjoint of $C\mathbb{E}_{(\cdot)}[\mathbf{X}]$ evaluated at λ is the same as the adjoint of $\mathbb{E}_{(\cdot)}[\mathbf{X}]$ evaluated at $C^T \lambda$.

The relevant conditions to apply this theorem are satisfied, as $(\mathcal{M}(\Omega), \|\cdot\|_{TV})$ and $(\mathbb{R}^d, \|\cdot\|_2)$ are Banach spaces and all conditions on the functions were verified save for the condition on the intersection of domains. To this effect, it was noted in Lem. 2 that the norm term is continuous on \mathbb{R}^d and in Lem. 1 that the divergence term is proper. Hence the relevant intersection is nonempty and the norm term will be continuous on this set. Finally, the primal-dual recovery formula of Thm. 1 is given explicit form by Lem 1, as it was shown that the unique element of $\text{argmax}_{x \in X} \{(x, A^* \bar{y}^*) - f(x)\} = \partial f^*(A^* \bar{y}^*)$ is

$$\bar{\rho}_\psi = \frac{\exp(\psi(x))q(x)}{\int_{\Omega} \exp(\psi(x))q(x) dx} dx.$$

Thus, evaluating $\bar{\rho}_{\langle C^T \bar{\lambda}, x \rangle}$ establishes the claim. \square

The utility of the dual problem is that it permits a staggering dimensionality reduction, passing from an infinite-dimensional problem to a finite-dimensional one. Moreover, the form of the dual problem makes precise the role of α in Eq. 3. Notably in [2, Cor. 4.9] the problem

$$(14) \quad \inf_{\rho \in \mathcal{P}(\Omega) \cap \text{dom } \mathcal{K}(\cdot, \mu)} \mathcal{K}(\rho, \mu) \quad \text{s.t.} \quad \|C\mathbb{E}_\rho[\mathbf{X}] - b\|_2^2 \leq \frac{1}{2\alpha}$$

is paired in duality with Eq. 12. Thus the choice of α is directly related to the fidelity of $C\mathbb{E}_\rho[\mathbf{X}]$ to the blurred image. The following section is devoted to the choice of a prior and describing a method to directly compute $\mathbb{E}_{\bar{\rho}}[\mathbf{X}]$ from a solution of 12.

3.3. Probabilistic Interpretation of Dual Problem. If no information is known about the original image, the prior μ is used to impose box constraints on the optimizer such that its expectation will be in the interval $[0, 1]^d$ and will only assign non-zero probability to measurable subsets of this interval. With this consideration in mind, the prior distribution should be the distribution of the random vector $\mathbf{X} = [X_1, X_2, \dots]$ with the X_i denoting independent random variables with uniform distributions on the interval $[u_i, v_i]$. If the k^{th} pixel of the original image is unknown, we let $[u_k, v_k] = [0 - \epsilon, 1 + \epsilon]$ for $\epsilon > 0$ small in order to provide a buffer for numerical errors.

However, if the k^{th} pixel of the ground truth image was known to have a value of ℓ , one can enforce this constraint by taking the random variable X_k to be distributed uniformly on $[\ell - \epsilon, \ell + \epsilon]$. Constructing μ in this fashion guarantees that its support (and hence Ω) is compact.

To deal with the integrals in Eq. 12 and Eq. 13 it is convenient to note that (cf. [21, Sec. 4.4])

$$\int_{\Omega} \exp(\langle C^T \lambda, x \rangle) q(x) dx = \mathbb{M}_{\mathbf{X}}[C^T \lambda],$$

the moment-generating function of \mathbf{X} evaluated at $C^T \lambda$. Since the X_i are independently distributed, $\mathbb{M}_{\mathbf{X}}[t] = \prod_{i=1}^d \mathbb{M}_{X_i}[t]$ [21, Sec. 4.4] and since the X_i are uniformly distributed on $[u_i, v_i]$ one has

$$\mathbb{M}_{\mathbf{X}}[t] = \prod_{i=1}^d \frac{e^{t_i v_i} - e^{t_i u_i}}{t_i (v_i - u_i)}$$

and therefore the dual problem with this choice of prior can be written as

$$(15) \quad \max_{\lambda \in \mathbb{R}^d} \left\{ \langle b, \lambda \rangle - \frac{1}{2\alpha} \|\lambda\|_2^2 - \sum_{i=1}^d \log \left(\frac{e^{C_i^T \lambda v_i} - e^{C_i^T \lambda u_i}}{C_i^T \lambda (v_i - u_i)} \right) \right\}.$$

An optimizer of Eq. 15 can be determined using a number of standard numerical solvers. We opted for the implementation [3] of the L-BFGS algorithm due to its speed and efficiency.

Since only the expectation of the optimal probability measure for Eq. 3 is of interest, we compute the i^{th} component of the expectation $(\mathbb{E}_{\bar{\rho}}[\mathbf{X}])_i$ of the optimizer provided by the primal-dual recovery formula Eq. 13 via

$$\frac{\int_{\Omega} x_i e^{\langle C^T \bar{\lambda}, x \rangle} q(x) dx}{\int_{\Omega} e^{\langle C^T \bar{\lambda}, x \rangle} q(x) dx} = \partial_{t_i} \log \left(\int_{\Omega} e^{\langle t, x \rangle} q(x) dx \right) \Big|_{t=C^T \bar{\lambda}}.$$

Using the independence assumption on the prior, we obtain

$$\mathbb{E}_{\bar{\rho}}[\mathbf{X}] = \nabla_t \sum_{i=1}^d \log(\mathbb{M}_{X_i}[t])$$

such that the best estimate of the ground truth image is given by

$$(16) \quad (\mathbb{E}_{\bar{\rho}}[\mathbf{X}])_i = \frac{v_i e^{C_i^T \bar{\lambda} v_i} - u_i e^{C_i^T \bar{\lambda} u_i}}{e^{C_i^T \bar{\lambda} v_i} - e^{C_i^T \bar{\lambda} u_i}} - \frac{1}{C_i^T \bar{\lambda}}.$$

With Eq. 15 and Eq. 16 in hand, our entropic method for deconvolution can be implemented.

3.4. Blind Deblurring. In order to implement blind deblurring on images that incorporate a symbology, one must first estimate the convolution kernel responsible for blurring the image. This step can be performed by analyzing the blurred symbolic constraints. We propose a method that is based on the entropic regularization framework discussed in the previous sections.

In order to perform this kernel estimation step, we will use the same framework as Eq. 3 with x playing the role of c . In the assumption that the kernel is of size $k \times k$, we take $\Omega = [0 - \epsilon, 1 + \epsilon]^{k^2}$ for $\epsilon > 0$ small (again to account for numerical error) and consider the problem

$$(17) \quad \inf_{\eta \in \mathcal{P}(\Omega)} \left\{ \frac{\gamma}{2} \|\mathbb{E}_\eta[\mathbf{X}] * x - b\|_2^2 + \mathcal{K}(\eta, \nu) \right\}.$$

Here, $\gamma > 0$ is a parameter that enforces fidelity and x, b are taken to be the segments of the original and blurred images which are fixed by the symbolic constraints. By analogy with Eq. 3, the expectation of the optimizer of Eq. 17 is taken to be the estimated kernel. The role of $\nu \in \mathcal{P}(\Omega)$ is to enforce the fact that the kernel should be normalized and non-negative (hence its components should be elements of $[0, 1]$). Hence we take its distribution to be the product of k^2 uniform distributions on $[0 - \epsilon, 1 + \epsilon]$. As in the non-blind deblurring step, the expectation of the optimizer of Eq. 17 can be determined by passing to the dual problem (which is of the same form as Eq. 15), solving the dual problem numerically and using the primal-dual recovery formula Eq. 16. A summary of the blind deblurring algorithm is compiled in Algorithm 1.

This method can be further refined to compare only the pixels of the symbology which are not convolved with pixels of the image which are unknown. By choosing these specific pixels, one can greatly improve the quality of the kernel estimate, as every pixel that was blurred to form the signal is known; however this refinement limits the size of convolution kernel which can be estimated.

Algorithm 1 Entropic Blind Deblurring

Input: Blurred image b , prior μ , kernel width k , fidelity parameters γ, α ;

Output: Deblurred image \bar{x}

$\nu \leftarrow$ density of k^2 uniformly distributed independent random variables

$\lambda_{\bar{c}} \leftarrow$ argmax of analog of Eq. 15 for kernel estimate.

$\bar{c} \leftarrow$ expectation of argmin of Eq. 17 computed via analog of Eq. 16 for kernel estimate evaluated at $\lambda_{\bar{c}}$

$\lambda_{\bar{x}} \leftarrow$ argmax of Eq. 15

$\bar{x} \leftarrow$ expectation of argmin of Eq. 3 with kernel \bar{c} computed via Eq. 16 evaluated at $\lambda_{\bar{x}}$

return \bar{x}

4. RESULTS

We present results obtained using our method on certain simulated images. We begin with deconvolution, i.e. when the blurring kernel c is known. Fig. 1 demonstrates the power of this method. Indeed, from even a highly blurred image, a near perfect estimate of the original image can be obtained provided the fidelity parameter α is sufficiently large

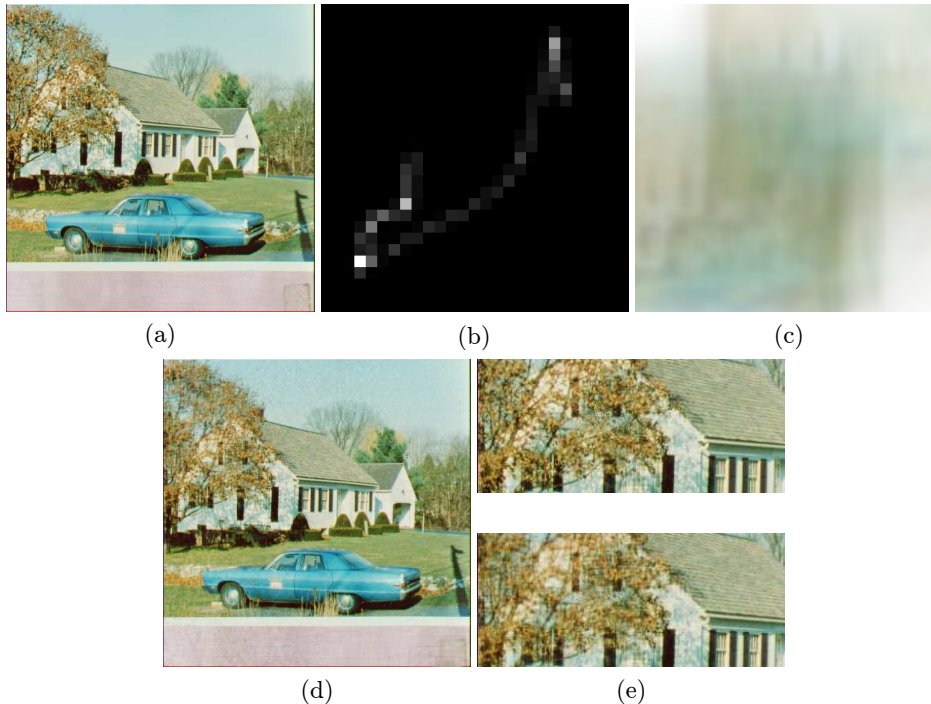


FIGURE 1. **Deconvolution:** (a) is the original image. (b) is the 459 pixel wide convolution kernel. (c) is the blurred image. (d) is obtained from the blurred image using the non-blind deblurring method. (e) compares the fine details of the original image (left) and deblurred image (right). Despite the high degree of blurring, the reproduction matches the original almost exactly. Comparisons to Krishnan and Fergus’s fast deconvolution method [10] and the expected patch log likelihood deconvolution method [28] were performed, but neither method converged with such a large kernel.

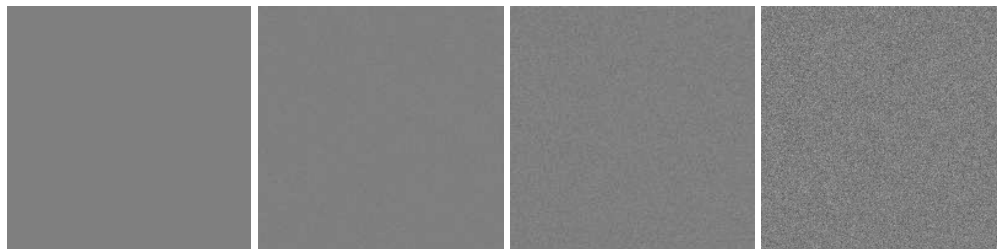


FIGURE 2. **Examples of Noise:** The leftmost image is a uniformly colored image. The image is subsequently degraded by 1%, 2% and 5% additive Gaussian noise in the centre left, center right and rightmost images respectively.

(in practice $\alpha = 10^{15}$ yields good results). Fig. 3 provides an example in which a blurry and noisy image has been deblurred using the non-blind deblurring method. We note that the method does not actively denoise blurred images, so a preprocessing step consisting of expected patch log likelihood (EPLL) denoising [28] is first performed. The resulting image is subsequently deblurred and finally TV denoising [22] is used to smooth the image. Note

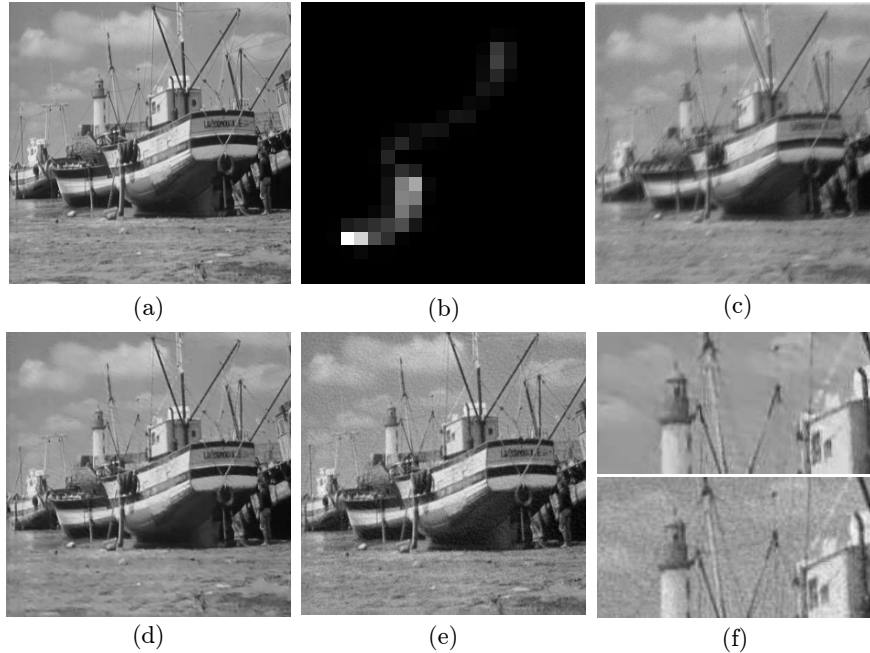


FIGURE 3. **Deconvolution with noise:** (a) is the original scene. (b) is the 23 pixel wide convolution kernel. (c) is the blurred image which is further degraded with 1% Gaussian noise. (d) is the result obtained from the blurred image via the non-blind deblurring method. (e) is the result obtained using Krishnan and Fergus’s fast deconvolution method [10]. (f) compares the fine detail of our result (top) and the result of the fast deconvolution method (bottom).

that for binary images such as text, TV denoising can be replaced by a thresholding step. Fig. 2 demonstrates the effects of different magnitudes of noise on a uniformly colored image.

Results for blind deblurring are compiled in Figs. 4 and 6. In this case $\gamma = 10^5$ and $\alpha = 10^6$ provide good results in the noiseless case and $\gamma = 10^3, \alpha = 10^4$ is adequate for the noisy case, but these parameters require manual tuning to yield the best results.

4.1. The Effects of Noise. In the presence of additive noise, attempting to deblur images using methods that are not tailored for noise is generally ineffective. Indeed, the image acquisition model $b = c * x$ is replaced by $b = c * x + n$ where n denotes the added noise. The noiseless model posits that the captured image should be relatively smooth due to the convolution, whereas the added noise sharpens segments of the image randomly, so the two models are incompatible. However, Figs. 3 and 4 show that our method yields good results in both deconvolution and blind deblurring when a denoising preprocessing step and a smoothing postprocessing step are utilized.

Remarkably, the blind deblurring method is more robust to the presence of additive noise in the blurred image. Indeed, accurate results were obtained with up to 5% Gaussian noise in the blind case whereas in the non-blind case, quality of the recovery diminished past 1% Gaussian noise. This is due to the fact that the preprocessing step fundamentally changes the blurring kernel of the image. We are therefore attempting to deconvolve the image with the wrong kernel, thus leading to aberrations. On the other hand, the estimated kernel

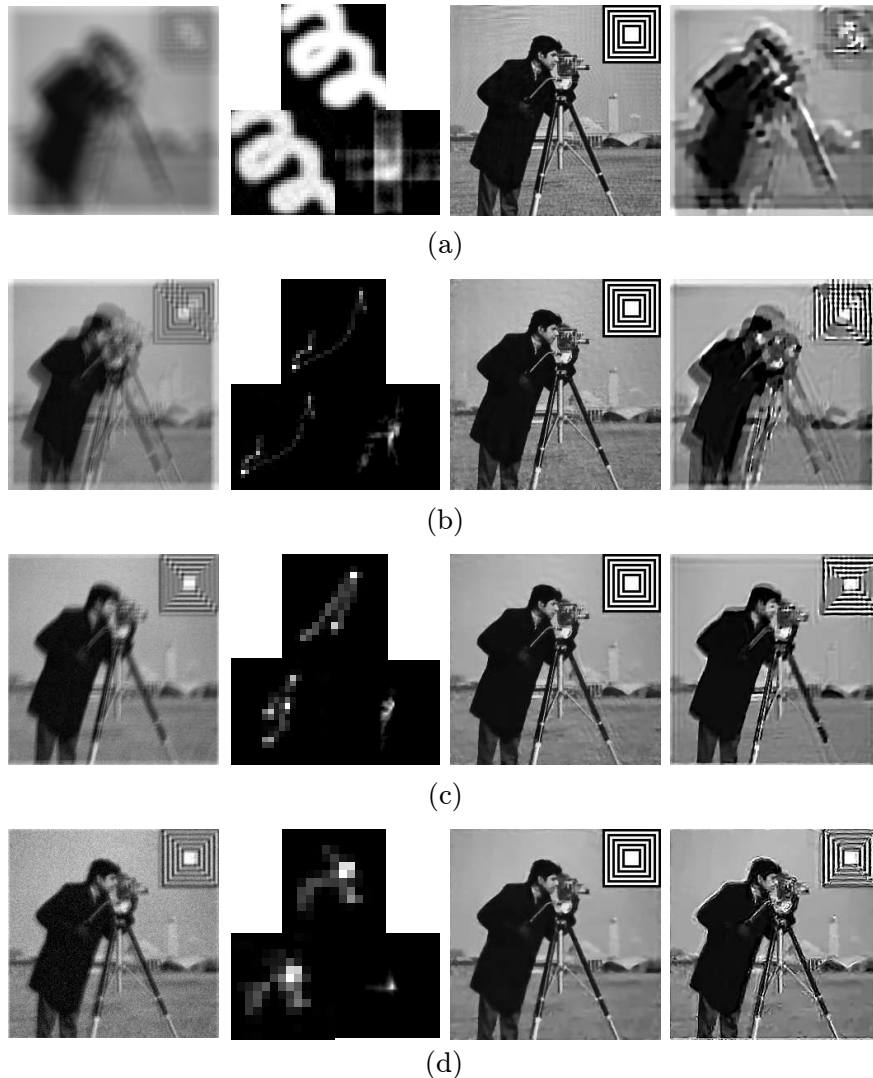


FIGURE 4. Blind deblurring with and without noise: This figure compares the performance of our blind deblurring method with EPLL denoising preprocessing and TV denoising postprocessing to that of Pan *et al.*'s blind deblurring method [15] with an EPLL denoising preprocessing step when deblurring images with varying amounts of noise and different blurring kernels. The subfigures are arranged as follows: **Left:** Blurred and noisy image. **Centre left:** Original convolution kernel on top, our estimated kernel in the bottom left and Pan *et al.*'s estimated kernel in the bottom right. **Centre right:** The latent image obtained by our method. **Right:** The latent image obtained by Pan *et al.*'s method (a) is noiseless with a 33 pixel wide kernel. (b) has 1% Gaussian noise with a 27 pixel wide kernel. (c) has 2% Gaussian noise with a 17 pixel wide kernel and (d) has 5% Gaussian Noise with a 13 pixel wide kernel. Of note is that our method is consistently smoother, the differences are best viewed on a high resolution monitor.

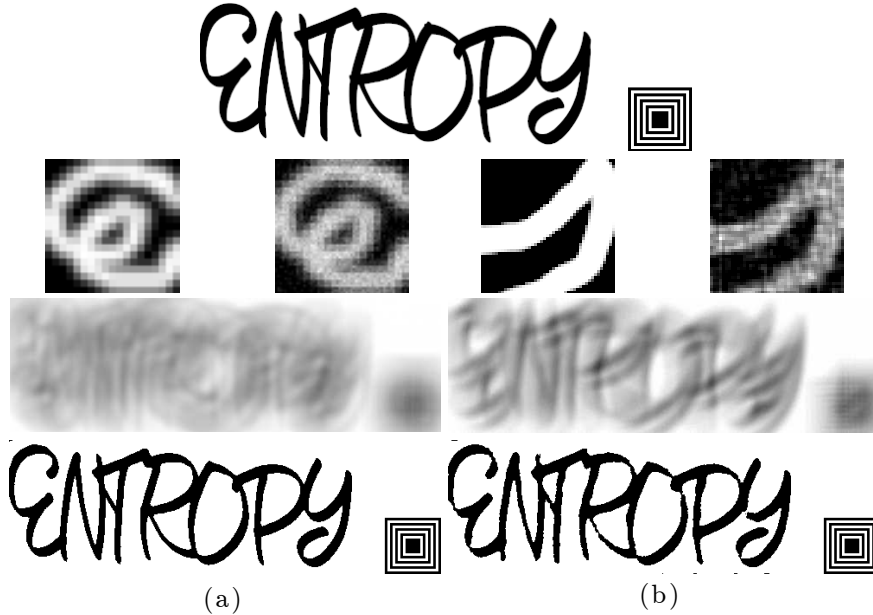


FIGURE 5. **Blind text deblurring with and without noise:** At the top is the original image. The subfigures are organised as follows: Top: Original convolution kernel on the right and estimated kernel on the left. Middle: Blurred and noisy image. Bottom: Deblurred image obtained using our method with an EPLL denoising preprocessing step and a thresholding postprocessing step. (a) is noiseless with a 57×57 pixel kernel. (b) has 1% Gaussian noise with a 45 pixel wide kernel.

for blind deblurring is likely to approximate the kernel modified by the preprocessing step, leading to better results. Moreover, a sparse (Poisson) prior was used in the kernel estimate for the results in Fig. 4 so as to mitigate the effects of noise on the symbology.

Finally, we note that there is a tradeoff between the magnitude of blurring and the magnitude of noise. Indeed, large amounts of noise can be dealt with only if the blurring kernel is relatively small and for large blurring kernels, only small amounts of noise can be considered. This is due to the fact that for larger kernels, deviations in kernel estimation affect the convolved image to a greater extent than for small kernels.

4.2. The Role of the Prior. The choice of prior μ is not limited to a product of uniform distributions. Indeed, depending on the situation, specialized priors can be constructed in order to better capture the underlying properties exhibited by the image. We provide as an example the use of Bernoulli priors to model binary data and of Poisson priors to model sparsity. Fig. 7 presents a comparison of deblurring a binary text images using different priors with the same choice of $\alpha = 2 \times 10^{11}$. In this case, sparsity has been used to promote the presence of a white background by inverting the colors of the channel during the deblurring process.

5. DISCUSSION

It is surprising that inference schemes of the type considered in this paper have not yet been applied to image deblurring. Indeed, the principle of maximum entropy was first

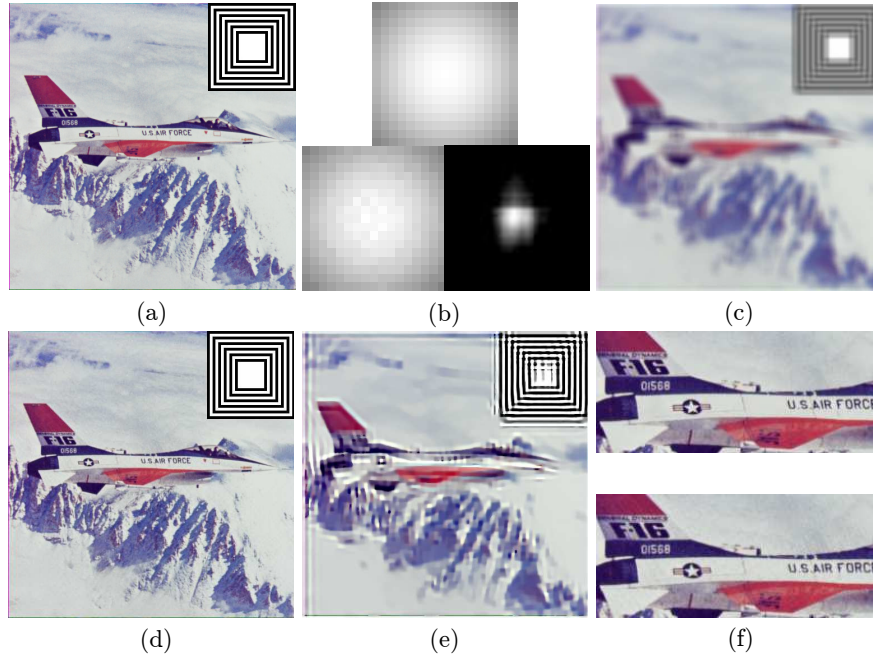


FIGURE 6. **Blind deblurring in color:** (a) is the original image. (b) compiles the original 17×17 pixel convolution kernel on top, our estimated kernel on the bottom left and the kernel obtained by Pan *et al.*'s method on the bottom right. (c) is the blurred image. (d) is the image obtained by performing blind deblurring on the previous blurred image using our method (without preprocessing or postprocessing). (e) is the image obtained via Pan *et al.*'s blind deblurring method. (d) demonstrates that the fine details of the original image (top) are preserved in our deblurred image (bottom).

developed in a pair of papers published by E.T. Jaynes in 1957. Furthermore, the theory of Fenchel-Rockafellar duality is well-established in the convex analysis literature and has found applications to solving maximum entropy estimation problems (cf. [6]).

Since our algorithm models blur as the convolution of the clean image with a single unknown blur kernel, it relies crucially on the spatial uniformity of the blur. This assumption may not hold in certain cases. For example, an image captured by a steady camera that contains a feature that moves during image capture will exhibit non-uniform motion blur. It may be of interest to explore extensions of this algorithm that divide the observed image into patches and estimate different blur kernels for each patch (cf. the motion flow approach proposed in [7])

Finally, our method is flexible with respect to the choice of prior. Indeed, any distribution with a tractable moment generating function may serve as a prior for the Kullback-Leibler divergence term in our primal problem. It would be interesting to consider using priors that encode global information regarding the latent image. For example, one might construct a class-specific prior that assigns high likelihood to images within a particular class (such as face images) and low likelihood to all other images (cf. [1]). A Gaussian mixture model trained on a particular class of images may serve as a useful prior for such purposes.

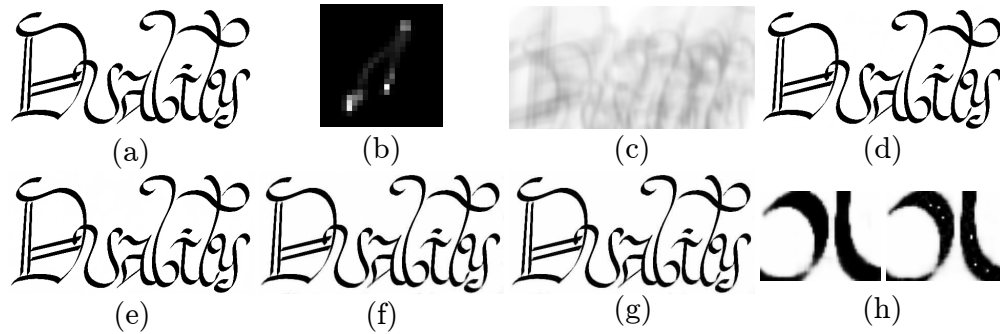


FIGURE 7. **Deconvolution with different priors:** (a) is the original binary text image. (b) is the 207×207 pixel convolution kernel. (c) is obtained by blurring the text with the convolution kernel. (d) and (e) are the results of performing deconvolution on the previous blurred image using Bernoulli and Poisson priors respectively using $\alpha = 10^{10}$. (f) and (g) were obtained by deconvolving with $\alpha = 10^6$ with the two priors. (e) presents the fine detail of the deconvolution with $\alpha = 10^6$ with the Bernoulli prior on the left and the Poisson prior on the right. Pixels which were black in the Bernoulli prior, but were gray in the Poisson prior have been made white manually in order to demonstrate the effect of a sparse prior.

IMPLEMENTATION DETAILS

All figures were generated by implementing the methods in the Python programming language using the Jupyter notebook environment. Images were blurred synthetically using motion blur kernels taken from [12] as well as Gaussian blur kernels to simulate out of focus blur. The relevant convolutions are performed using fast Fourier transforms. Images that are not standard test bank images were generated using the GNU Image Manipulation Program (GIMP), moreover this software was used to add symbolic constraints to images that did not originally incorporate them. All testing was performed on a laptop with an Intel i5-4200U processor. The running time of this method depends on a number of factors such as the size of the image being deblurred, whether the image is monochrome or color, the desired quality of the reproduction desired (controlled by the parameter α) as well as the size of the kernel and whether or not it is given. If a very accurate result is required, these runtimes vary from a few seconds for a small monochrome text image blurred with a small sized kernel to upwards of an hour for a highly blurred color image.

REFERENCES

1. S. Anwar, C. Phuoc Huynh, and F. Porikl, *Image Deblurring with a Class-Specific Prior*, IEEE Trans. on Pattern Anal. Mach. Intell. **41** (2019), 2112–2130. [13](#)
2. J.M. Borwein and A.S. Lewis, *Partially finite convex programming, Part I: Quasi relative interiors and duality theory*, Math.l Program. **57** (1992), 15–48. [6](#)
3. R.H. Byrd, P. Lu, J. Nocedal, and C. Zhu, *A Limited Memory Algorithm for Bound Constrained Optimization*, SIAM J. Sci. Comput. **16** (1995), 1190–1208. [7](#)
4. T. M. Cover and J. A. Thomas, *Elements of Information Theory*, Wiley, 2006. [5](#)
5. J.-D. Deuschel and D. W. Stroock, *Large Deviations*, Academic Press, 1989. [4](#)

6. M. Dudik, S.J. Philips, and R.E. Schapire, *Maximum Entropy Density Estimation with Generalized Regularization and an Application to Species Distribution Modeling*, Journal of Machine Learning Research **8** (2007), 1217–1260. [13](#)
7. D. Gong, J. Yang, L. Liu, Y. Zhang, I. Reid, C. Shen, A. Hengel, and Q. Shi, *From motion blur to motion flow: a deep learning solution for removing heterogeneous motion blur*, CPVR 2016 (2016). [13](#)
8. E. T. Jaynes, *Information Theory and Statistical Mechanics*, Phys. Rev. **106** (1957), 620–630. [1](#)
9. ———, *Information Theory and Statistical Mechanics. II*, Phys. Rev. **108** (1957), 171–190. [1](#)
10. D. Krishnan and R. Fergus, *Fast image deconvolution using hyper-laplacian priors*, NIPS 2009 (2009), 1033–1041. [9](#), [10](#)
11. O. Kupyn, V. Budzan, M. Mykhailych, D. Mishkin., and J. Matasi, *DeblurGAN: Blind Motion Deblurring Using Conditional Adversarial Networks*, CVPR 2018 (2018), 8183–8192. [2](#)
12. A. Levin, Y. Weiss, F. Durand, and W.T. Freeman, *Understanding and Evaluating Deconvolution Algorithms*, CVPR 2009 (2009), 1964–1971. [14](#)
13. S. Nah, T.H. Kim, and K.M. Lee, *Deep Multi-scale Convolutional Neural Network for Dynamic Scene Deblurring*, CVPR 2017 (2017), 3883–3891. [2](#)
14. M. Noroozi, P. Chandramouli, and P. Favaro, *Motion Deblurring in the Wild*, GCPR 2017 (2017), 65–77. [2](#)
15. J. Pan, Z. Hu, Z. Su, and M.-H. Yang, *L_0 -Regularized Intensity and Gradient Prior for Deblurring Text Images and Beyond*, IEEE Trans. Pattern Anal. Mach. Intell. **39** (2017), no. 2, 342–355. [2](#), [11](#)
16. J. Pan, D. Sun, H. Pfister, and M.-H. Yang, *Blind Image Deblurring Using Dark Channel Prior*, CVPR 2016 (2016), 1628–1636. [2](#)
17. S. Ramakrishnan, S. Pachori, A. Gangopadhyay, and S. Raman, *Deep Generative Filter for Motion Deblurring*, ICCV 2017 (2017), 2993–3000. [2](#)
18. W. Ren, X. Cao, J. Pan, X. Guo, W. Zuo, and M.-H. Yang, *Image Deblurring via Enhanced Low-Rank Prior*, IEEE Trans. Image Process. **25** (2016), no. 7, 3426–3437. [2](#)
19. G. Rioux, C. Scarvelis, R. Choksi, T. Hoheisel, and P. Maréchal, *Blind Deblurring of Barcodes via Kullback-Leibler Divergence*, IEEE Trans. Pattern Anal. Mach. Intell., in press (2019), doi: [10.1109/TPAMI.2019.2927311](#). [1](#), [2](#)
20. R.T. Rockafellar and R. J-B Wets, *Variational Analysis*, Springer, 2009. [5](#)
21. V.K. Rohatgi and A.K. MD. E. Saleh, *An Introduction to Probability and Statistics*, Wiley, 2001. [7](#)
22. L. Rudin, S. Osher, and E. Fatemi, *Nonlinear total variation based noise removal algorithms*, Physica D **60** (1992), 259–268. [9](#)
23. W. Rudin, *Real and Complex Analysis*, McGraw-Hill, 1987. [4](#), [5](#)
24. C.J. Schuler, M. Hirsch, S. Harmeling, and B. Schölkopf, *Learning to Deblur*, IEEE Trans. Pattern Anal. Mach. Intell. **38** (2015), no. 7, 1439–1451. [2](#)
25. X. Tao, H. Gao, X. Shen, J. Wang, and J. Jia, *Scale-Recurrent Network for Deep Image Deblurring*, CVPR 2018 (2018), 8174–8182. [2](#)
26. A.N. Tikhonov and V.Y. Arsenin, *Solutions of Ill-Posed Problems*, Winston and Sons, 1977. [2](#)
27. C. Zălinescu, *Convex Analysis in General Vector Spaces*, World Scientific, 2002. [3](#), [4](#), [5](#)
28. D. Zoran and Y. Weiss, *From Learning Models of Natural Image Patches to Whole Image Restoration*, ICCV 2011 (2011), 479–486. [1](#), [9](#)